Cosmogenic nuclides constrain surface fluctuations of an East Antarctic outlet glacier since the Pliocene

Jones, R.S. [a-c*], Norton, K.P. [b], Mackintosh, A.N. [a,b], Anderson, J.T.H. [d,e], Kubik, P. [f], Vockenhuber, C. [f], Wittmann, H. [g], Fink, D. [h], Wilson, G.S. [d,e], Golledge, N.R. [a,i], McKay, R. [a]

[a] *Antarctic Research Centre, Victoria University of Wellington, PO Box 600, Wellington 6140, New Zealand*

[b] *School of Geography, Environment and Earth Sciences, Victoria University of Wellington, PO Box 600, Wellington 6140, New Zealand*

[c] *Department of Geography, Durham University, Science Laboratories, South Road, Durham, DH1 3LE, United Kingdom*

[d] *Geology Department, University of Otago, PO Box 56, Dunedin 9054, New Zealand*

[e] *Department of Marine Science, University of Otago, 310 Castle Street, Dunedin 9016, New Zealand*

[f] *Laboratory of Ion Beam Physics, ETH Zurich, Otto Stern Weg 5, 8093 Zurich, Switzerland*

[g] *Helmholtz-Zentrum Potsdam, GFZ Deutsches GeoForschungszentrum, Telegrafenberg, 14473 Potsdam, Germany*

[h] *Australian Nuclear Science and Technology Organization (ANSTO), Menai 2234, New South Wales, Australia*

[i] *GNS Science, Avalon, Lower Hutt, New Zealand*

[*] *Present address: Department of Geography, Durham University, United Kingdom (richard.s.jones@durham.ac.uk)*

Abstract

Understanding past changes in the Antarctic ice sheets provides insight into how they might respond to future climate warming. During the Pliocene and Pleistocene, geological data show that the East Antarctic Ice Sheet responded to glacial and interglacial cycles by remaining relatively stable in its interior, but oscillating at its marine-based margin. It is currently not clear how outlet glaciers, which connect the ice sheet interior to its margin, responded to these orbitally-paced climate cycles. Here we report new ice surface constraints from Skelton Glacier, an outlet of the East Antarctic ice sheet, which drains into the Ross Ice Shelf. Our multiple-isotope (^{10}Be and ^{26}Al) cosmogenic nuclide data indicate that currently ice-free areas adjacent to the glacier underwent substantial periods of exposure and ice cover in the past. We use an exposure-burial model driven by orbitally-paced glacial-interglacial cycles to determine the probable ice surface history implied by our data. This analysis shows that: 1) the glacier surface has likely fluctuated since at least the Pliocene; 2) the ice surface was >200 m higher than today during glacial periods, and the glacier has been thicker than present for ~75–90% of each glacial-interglacial cycle; and 3) ice cover at higher elevations possibly occurred for a relatively shorter time per Pliocene cycle than Pleistocene cycle. Our multiple-nuclide approach demonstrates the magnitude of ice surface fluctuations during the Pliocene and Pleistocene that are linked to marine-based ice margin variability.

Keywords

Antarctica; ice sheet; cosmogenic nuclides; Pliocene; Pleistocene; paleoclimate

1. Introduction

Geological records from ice-free areas of Antarctica can provide direct constraints on the sensitivity of the Antarctic ice sheet to past climatic changes. Nunataks that protrude through the ice serve as gauges of past ice sheet thickness change (e.g. Ackert et al., 1999; Stone et al., 2003). The production of *in situ* cosmogenic nuclides in a rock surface can be exploited to quantify whether and when ice previously overrode the area. In locations where this ice was predominantly cold-based, with little or no erosion of the rock surface, multiple-isotope measurements allow the long-term glacial history at the site to be explored (e.g. Balco et al., 2014; Bierman et al., 1999; Corbett et al., 2016; Lilly et al., 2010; Sugden et al., 2005); the nuclides ^{10}Be and ^{26}Al are produced in quartz at a constant ratio during periods of exposure, but the shorter half-life of ^{26}Al (0.716 Ma) relative to ^{10}Be (1.39 Ma) enables faster decay during periods of burial by ice, lowering the ratio of ^{26}Al to ^{10}Be (Lal, 1991). A rock surface with an old apparent exposure age from only a single nuclide indicates the minimum time since first exposed, but exposure may have been constant or intermittent over this time. Multiple-isotope measurements are required to determine if there has been a complex exposure history. A "simple" exposure history could be inferred if exposure ages are consistent between multiple nuclides, indicating constant exposure since first exposed. Whereas, a "complex" exposure history would result in exposure ages that are not consistent between multiple nuclides, indicating some period of burial since first exposed.

Multiple-isotope surface-exposure data, collected from near to the interior of the East Antarctic ice sheet (EAIS), have typically provided concentrations and ages consistent with a constant exposure history since first uncovered by ice. These ages show that first exposures were at times during the Pliocene, implying that the ice surface was higher than today in the Pliocene and has not been as high since then (e.g. Balco et al., 2014; Lilly et al., 2010; Yamane et al., 2015). Meanwhile, sediment cores drilled on the continental shelf reveal that

large-scale orbitally-paced oscillations of the ice margin occurred through the Pliocene and Pleistocene in marine-based portions of the ice sheet (e.g. drill core site AND-1B; McKay et al., 2012; Naish et al., 2009; Patterson et al., 2014), contemporaneous with local and global environmental changes (Levy et al., 2012). Outlet glaciers link such regions of contrasting ice sheet variability, controlling the flux of ice from the interior to the ice margin. Currently, we lack data constraining the behavior of outlet glaciers prior to the last glacial cycle, in the Pliocene and Pleistocene.

We report new multiple-isotope (^{10}Be and ^{26}Al) surface-exposure data from Skelton Glacier, an outlet of the EAIS. Here ice flows, through the Transantarctic Mountains, from the East Antarctic plateau to the Ross Sea embayment and over the AND-1B drill site (Talarico et al., 2012) (**Fig. 1**). Skelton Glacier is therefore suitably located to investigate the degree to which past oscillations of the marine-based ice margin that are documented at AND-1B propagated inland. Any past changes near the ice margin should have been expressed upstream as ice surface elevation changes, but the distance upstream and the magnitude of such changes during the Pliocene and Pleistocene is not well understood.

In this paper we determine whether the surface of Skelton Glacier was higher in the past, for how long and by how much it fluctuated, and whether such changes in ice surface elevation can be explained by glacial-interglacial oscillations of the ice margin. We apply an exposure-burial model to robustly evaluate the ice surface history implied by our cosmogenic nuclide data. The results of glacier flowline simulations that were constrained by geological and climatological data, presented in an associated study (Jones et al., 2016, and references therein), are then used to help better understand how glacier surface elevation changes corresponded to shifting ice dynamics under past contrasting climates.

2. Methods

2.1. Study area and sample collection

Six nunataks (Clinker Bluff, Halfway Nunatak, Névé Nunatak, Tate Peak, the Escalade Peak saddle with Tate Peak, and an unnamed nunatak) were targeted to provide spatial coverage of past ice surface changes (**Fig. 1**). Clinker Bluff, Halfway Nunatak and Névé Nunatak extend upstream from the modern grounding-line, adjacent to and north of the main flow path. Tate Peak, the Escalade Peak saddle and an unnamed nunatak are located to the south of the main flow path of Skelton Glacier, near to the ice divide with Mulock Glacier. The sample sites represent a range of elevations between approximately 2 m and 215 m above the adjacent ice surface, allowing relative changes in the past thickness of Skelton Glacier to be investigated.

The bedrock underlying the Skelton Glacier catchment is comprised of a metasedimentary basement (Skelton Group), overlain by sandstone sedimentary sequences (Beacon Supergroup), which are intruded by dolerite dykes and sills (Ferrar Supergroup) (Gunn and Warren, 1962). Névé Nunatak is made up of dolerite, Clinker Bluff is granite, Halfway Nunatak is comprised of both dolerite and granite, the unnamed nunatak consists of sandstone, and Tate and Escalade Peaks are predominantly comprised of sandstone and dolerite. Sandstone also likely underlies large parts of the upper catchment, which is evident from ice-free outcrops either side of The Portal, upstream of Névé Nunatak (**Fig. 1**).

Evidence of subaerial weathering and past overriding of ice is evident at each of these nunataks (**see supplementary Fig. 1**). Extensive, long-term surface weathering can be inferred from granite surfaces that are heavily spalled and large areas of exposed dolerite that are heavily fractured. However, past glacial activity is also apparent, as glacially-polished granite surfaces at Clinker Bluff and striated sandstone surfaces at Tate Peak, the Escalade Peak saddle and the unnamed nunatak, as well as perched boulders, erratic cobbles and

glacial till at Halfway and Névé Nunataks. Most clasts found strewn over these surfaces (including boulders >1 m in diameter) are sub-angular and derived from local bedrock, while erratic sandstone clasts, sourced from upstream, are less common. The geomorphology observed at these sites suggests both the preservation of weathered relict surfaces and the deposition of clasts at times of largely non-erosive ice cover.

Glacier flowline modeling, driven by available paleoclimate data, support our interpretations of the geomorphology. This modeling indicates that Skelton Glacier likely experienced warm-based ice with substantial basal sliding and erosion of the bed in overdeepenings within the central flow path, but minimal erosion elsewhere, during both Pliocene and Quaternary climates (Jones et al., 2016). The modeling suggests that 1) erratic cobbles, for example, those found at Halfway and Névé Nunataks, were likely sourced from beneath the warm-based areas, where subglacial erosion is predicted, before being transported to the less-erosive flanks of Skelton Glacier, and 2) any ice cover of the nunataks during the Pliocene and Quaternary was likely by ice with limited erosion potential, which is supported by the presence of angular to sub-angular clasts strewn over largely weathered bedrock surfaces, and well-developed patterned ground on some low gradient nunatak slopes. A bedrock surface sampled at these nunataks should, therefore, record a long-term glacial history, while an erratic cobble should record either recent exposure since it was last covered by ice or repeated exposure and burial since it was initially exposed at the nunatak.

In total, twelve samples were collected for surface-exposure analysis, from nunatak areas where there was evidence of past ice cover and away from areas of patterned ground. Samples were selected that had intact rock surfaces and signs of at least minor glacial abrasion, including 7 erratic sandstone cobbles on thin (<5 cm), compacted till that was draped over bedrock at Névé Nunatak, an isolated unweathered sandstone erratic boulder on bedrock at Halfway Nunatak, sandstone bedrock surfaces at the unnamed nunatak, Tate Peak

and Escalade Peak saddle, and a granite bedrock surface at Clinker Bluff (**Figs. 1 and 2, and supplementary Table 1 and Fig. 2**).

2.2. Sample processing, measurement, and exposure age calculation

Samples were prepared and beryllium and aluminum were extracted at Victoria University of Wellington (VUW), the University of Otago (UoO) and the Australian Nuclear Science and Technology Organisation (ANSTO) (**Table 1**), following established procedures (Mifsud et al., 2013; Norton et al., 2008; Von Blanckenburg et al., 1996). They were then measured for ^{10}Be and ^{26}Al at ETH Zurich and ANSTO for the samples processed at VUW and UoO/ANSTO, respectively. The ^{10}Be samples measured at ETH Zurich were normalized relative to the nominal ^{10}Be/^{9}Be value of 28.1×10^{-12} for S2007N, and at ANSTO to the nominal ^{10}Be/^{9}Be value of 8.56×10^{-12} for 07KNSTD-01-5-2 (Nishiizumi et al., 2007). The ^{26}Al samples measured at ETH Zurich were normalized relative to the nominal ^{26}Al/^{27}Al value of 48×10^{-11} for ZAL94N, and at ANSTO to the nominal ^{26}Al/^{27}Al value of 3.096×10^{-11} for KN-01-4-2 (Nishiizumi, 2004). All final AMS ^{10}Be/^{9}Be and ^{26}Al/^{27}Al values were corrected by their corresponding full chemistry procedural blanks. Final AMS isotopic ratios were converted to ^{10}Be and ^{26}Al concentrations (atoms g^{-1}) by using the measured ^{9}Be concentrations in the 372.5 ppm spike solution, and ICP-OES ^{27}Al assay in the quartz at GeoForschungsZentrum (GFZ) and ANSTO for samples processed at VUW and UoO/ANSTO respectively. The ICP-OES analyses performed at GFZ were replicated on ICP-MS at VUW, with measurements consistent at 1 sigma level and corresponding mean ^{26}Al concentrations differing by ~1–6%.

Surface-exposure ages were calculated from the measured concentrations of ^{10}Be and ^{26}Al, corrected for topographic shielding, sample thickness, rock density and an Antarctic atmospheric pressure gradient, using CRONUS-Earth online calculator (Balco et al., 2008).

They are termed ‘apparent exposure ages’ as they assume continuous exposure since initially exposed and near-zero surface erosion over that time.

2.3. Multiple-nuclide exposure-burial modeling

In order to better determine the ice surface history implied by the data, nuclide concentrations can be modeled through periods of exposure and burial (e.g. Balco et al., 2014; Bierman et al., 1999; Corbett et al., 2016; Sugden et al., 2005). Our approach assumes: 1) the episodes of past exposure and burial relate directly to fluctuations of the ice surface elevation; 2) these fluctuations occurred over uniform glacial-interglacial cycles (40-ka or 100-ka), as recorded by benthic oxygen isotopes and Antarctic marine sediments; and 3) the glacier surface elevation rose (i.e. sample burial) during glacial episodes, in response to buttressing near the terminus from expanded grounded ice in the Ross Sea (e.g. Denton and Hughes, 2000), and lowered (i.e. sample exposure) during interglacial episodes (**Fig. 3A**).

The concentration (atoms g^{-1}) of a nuclide in a rock surface (N_k) can be calculated for a glacial and an interglacial period as follows:

$$N_k^i = N_k^{i-1}\, exp\left[-\left(\lambda_k + \frac{\rho\ \varepsilon_{sg}}{\Lambda}\right) t_b\right] \quad (1)$$

and

$$N_k^i = N_k^{i-1}\, exp\left[-\left(\lambda_k + \frac{\rho\ \varepsilon_{sa}}{\Lambda}\right) t_e\right] + \frac{P_k}{\lambda_k + \frac{\rho\ \varepsilon_{sa}}{\Lambda}}\left(1 - exp\left[-\left(\lambda_k + \frac{\rho\ \varepsilon_{sa}}{\Lambda}\right) t_e\right]\right) \quad (2)$$

where P_k is the production rate (atoms g^{-1} a^{-1}) and λ_k is the decay constant (a^{-1}) for nuclide k, ρ is the rock density (g cm^{-3}), ε_{sg} and ε_{sa} are the subglacial and subaerial erosion rates (cm a^{-1}), Λ is the attenuation length (g cm^{-2}), and t_b and t_e are the durations of burial and exposure per glacial-interglacial cycle. Nuclide concentrations calculated during each glacial or

interglacial period (N_k^i) are dependent on the on the concentrations calculated for the preceding glacial or interglacial period (N_k^{i-1}).

Nuclide concentrations are zero at the start of an exposure-burial scenario (t_{total}), and a forward model calculates concentrations as stated in Equations 1 and 2 iteratively over glacial-interglacial cycles until present day (**Fig. 3**). The model uses the decay constants of 4.99 x 10^{-7} a^{-1} for ^{10}Be and 9.83 x 10^{-7} a^{-1} for ^{26}Al (Chmeleff et al., 2010; Korschinek et al., 2010; Nishiizumi, 2004), an attenuation length of 160 g cm^{-2} (Balco et al., 2008) and a rock density of 2.65 g cm^{-3}. Production is calculated for spallation using the ^{10}Be production rate of 4.49 atoms g a^{-1}, predicted by a global calibration dataset (Balco et al., 2008). While this value may slightly overestimate the true production rate, this analysis relies primarily on the measured decay constants and the commonly used ^{26}Al/^{10}Be production ratio of 6.75 (Balco and Shuster, 2009). Production by muons is small (~1.5–2% that of spallation), and is therefore considered negligible (e.g. Balco et al., 2014; Briner et al., 2006; Lilly et al., 2010). The resulting nuclide concentrations are then normalized by the Sea-Level-High-Latitude production rate (Balco et al., 2008; Stone, 2000) for comparison with measured concentrations that are normalized by their site-specific production rate.

Nuclide concentrations evolve in the model along exposure/burial pathways according to the periodicity of glacial-interglacial cycles (t_{cycle}), percent buried per cycle ($\%\ bur$), subaerial erosion rate (ε_{sa}), subglacial erosion rate (ε_{sg}), and amount of total exposure/burial time (t_{total}) (**Fig. 3**). An additional parameter, the duration of constant exposure prior to cyclic exposure-burial (t_{pre}), is used only for cobble samples. These parameters are either specified or allowed to float between given ranges of values for each model simulation (**supplementary Table 2**), which we proceed to explain below.

We assume that the cyclicity in exposure and burial is driven by the dominant orbital cycle reflected in benthic oxygen isotopes, which reflect ocean temperature and global ice

volume (Lisiecki and Raymo, 2005). Similar orbital frequencies are recorded in Antarctic offshore sediment cores, including at drill site AND-1B downstream of Skelton Glacier, representing oscillations of the ice margin since at least the Pliocene (McKay et al., 2012; Naish et al., 2009; Patterson et al., 2014). Based on these records, we impose t_{cycle} values of 40 ka during the Pliocene (5.4–2.6 Ma BP) and 100 ka during the Late Pleistocene (0.8–0 Ma BP). The cycle periodicity is less certain during the intervening Early-Mid Pleistocene (2.6–0.8 Ma BP). We therefore set t_{cycle} as either 40 ka or 100 ka for this period, meaning that half of all simulations use either 40-ka or 100-ka cycles during the Early-Mid Pleistocene. For scenarios where initial exposure occurs prior to the Pliocene, concentrations evolve according to 20-ka, 40-ka or 100-ka cycles until 5.4 Ma BP. However, in this study we focus on the Pliocene to present-day, when the ice surface history implied by our data can be predicted more reliably.

The percentage of a glacial-interglacial cycle that a rock surface was ice-covered likely varied depending on the sample location (e.g. elevation of the site above the modern ice surface), and therefore we use a range of 0–100% (in 5% increments) ice cover per cycle (% bur) in the model (**Fig. 3A**); as an example, 60 % bur of a Late Pleistocene cycle (t_{cycle} = 100 ka) equates to 40 ka exposed (t_e) and 60 ka buried (t_b). Full shielding by ice, and therefore zero nuclide production, is assumed during glacial periods, while no cover of the rock surface, zero shielding and full nuclide production is assumed during interglacial periods. Today, snow cover is thin and temporary at nunataks because of low moisture transport, low albedo and high winds, and till deposition at these sites is minimal (**see supplementary Fig. 1**), and therefore partial shielding during interglacial periods is considered negligible.

In addition to radionuclide decay, nuclides can be lost to subaerial (ε_{sa}) or subglacial (ε_{sg}) erosion, during exposure or burial, respectively. The model uses a range of possible

erosion rates (0–1.5 m Ma^{-1}, in 0.1 m Ma^{-1} increments), partly constrained by available data from Antarctica that imply rates less than 1.5 m Ma^{-1} (e.g. Balco et al., 2014; Ivy-Ochs et al., 1995). These are independently applied at constant rates during periods of burial and exposure, as described in equations 1 and 2 respectively; the effects of subglacial erosion on nuclide concentrations following a period of exposure are highlighted in **Fig. 3B**. While we assume that surface erosion is steady, there was no evidence of large-scale episodic erosion, such as plucking, of rock surfaces at the sample sites.

The rock surfaces could have been buried and exposed over many millions years or just the last glacial-interglacial cycle, with the total recorded exposure/burial history partly dependent on the amount of cumulative erosion; higher erosion rates cause nuclide concentrations to reach equilibrium more rapidly, limiting the signal of past ice surface fluctuations that can be preserved (Balco et al., 2014). We include a large range of t_{total} in the model (0–8 Ma BP, in 10-ka increments), with the longer histories limited by the erosion rate for each modeled scenario.

While the bedrock samples can be assumed to have undergone *in situ* exposure and burial, the erratic samples collected at Névé Nunatak could have a more diverse history. There is a chance that some of these cobbles were exposed upstream for some time prior to being deposited at Névé Nunatak and subsequent cycles of exposure and burial. To account for this possibility, the concentrations are allowed to evolve from constant exposure for t_{pre}, prior to cyclic exposure-burial in the model; the concentrations resulting from these scenarios are only compared to the cobble samples from Névé Nunatak.

Nuclide concentrations were modeled through time for each combination of parameter values. Scenarios were then only accepted where the final nuclide concentrations matched the measured sample concentrations, using a uniform uncertainty distribution for each measurement (at 95% confidence; measurement uncertainty). It is worth noting here that the

uncertainty of the measurements therefore partly governs the ability of these types of modeling approaches to identify simulated scenarios consistent with the data. In the case of the erratic cobbles, we only want to simulate the exposure-burial history at Névé Nunatak, where the multiple samples must have undergone the same ice surface fluctuations for at least some period of time and, therefore, we additionally only accepted scenarios of exposure/burial time (% bur and t_{cycle}) if they were consistent between all Névé Nunatak samples. The resulting frequency populations were then converted to probability estimates to identify the most likely ice cover history implied by the samples.

3. Results

3.1. Apparent exposure ages and two-isotope analysis

Surface-exposure ages were calculated from measured nuclide concentrations as described above for all samples (**Tables 1 and 2**). The youngest (^{10}Be) exposure age comes from an erratic boulder with a relatively unweathered surface at Halfway Nunatak (HN36), dated to 5.8 ± 0.8 ka BP. This is the only sample that most likely records ice surface lowering during the last glacial cycle.

All other samples provide ^{10}Be and ^{26}Al apparent exposure ages in the range of ~90 ka to 1 Ma BP (**Fig. 4A**), which are broadly older for samples at higher elevations. Critically, the ages derived from ^{10}Be and ^{26}Al isotopes are not consistent for any of these samples (**Fig. 4A**). The lack of agreement between the two isotopes indicates that the samples record the inheritance of cosmogenic nuclides, representing at least one episode of exposure prior to the last episode of burial (**Fig. 3B**). Therefore, while these apparent exposure ages cannot be considered absolute estimates for the timing of deglaciation, we can learn about the exposure and burial histories of these samples by evaluating their multiple nuclide concentrations.

Nuclide concentrations range from $2.1 \times 10^6 \pm 6 \times 10^4$ atoms g^{-1} to $1.5 \times 10^7 \pm 4 \times 10^5$ atoms g^{-1} and $1.1 \times 10^7 \pm 6 \times 10^5$ atoms g^{-1} to $6.3 \times 10^7 \pm 2 \times 10^6$ atoms g^{-1}, for ^{10}Be and ^{26}Al respectively (at 1 σ) (**Table 2**). These values correspond to mean $^{26}Al/^{10}Be$ ratios of 3.79 to 5.48, which are significantly below the production ratio of 6.75 (Balco and Shuster, 2009). The relative position of these nuclide concentrations (normalized to production rates) on a two-isotope plot provides a preliminary assessment of the degree of exposure and burial experienced by the samples (**Fig. 4B**). A sample that has experienced continuous exposure and any degree of subaerial erosion will plot within the steady-state erosion island (shown as a bold black line), while a sample with concentrations plotting below this island indicates that the sample must have experienced burial following initial exposure, the minimum amount of which is denoted by isochrones of equal burial time. It is also possible for a sample that has undergone exposure and burial to plot within the steady-state erosion island, if the cumulative burial time is sufficiently less than that of exposure, and erosion is minimal. The amount of burial time implied by this plot is largely determined by the $^{26}Al/^{10}Be$ ratio, which has a relatively large uncertainty because of error propagation from both isotope concentrations, with generally greater uncertainty for ^{26}Al than ^{10}Be measurements.

Our samples record a long time of cumulative exposure and burial, which varies in magnitude between samples and sites (**Fig. 4B**). Two samples at Névé Nunatak (NN33c and NN33d) plot within the steady-state erosion island, given the measurement uncertainty of the nuclide concentrations. These samples could possibly be explained by continuous exposure and erosion since first deposited, but this is unlikely considering that these samples would have shared at least some exposure/burial history with neighboring samples at Névé Nunatak, which indicate significant burial similar to the other sites. The simplest scenario for all of our samples is that they underwent a single period of continuous exposure, ranging from ~150 ka to ~1.8 Ma (at 1 σ), followed by a single period of continuous burial, ranging from ~100 ka to

~850 ka (at 1 σ) (**Fig. 4B**). This would imply a switch from uninterrupted ice-free conditions to uninterrupted ice cover during the Pleistocene, with the time that this occurred varying between samples and sites. Such a simple two-stage (exposure then burial) history is unlikely as it ignores potential surface erosion and cyclic episodes of ice cover, which is recorded for the ice margin downstream at the AND-1B core site (McKay et al., 2012; Naish et al., 2009). This scenario also ignores the data from Halfway Nunatak, which implies a recent re-exposure period since at least ~5.8 ka BP. In order to robustly determine the history of past ice surface fluctuations reflected in the samples, a more systematic analysis of the potential exposure-burial histories is required.

3.2. Exposure-burial modeling of long-term ice surface fluctuations

We explored this long-term history further by modeling the evolution of nuclide concentrations through glacial-interglacial cycles. By accepting the simulated nuclide concentrations that matched our data, we can identify which exposure-burial scenarios are consistent with our samples (**Fig. 5**). The total exposure-burial history recorded by the samples can be inferred from the distribution of modeled time since first exposed (**Fig. 6A**). Based on the modes and 68% confidence bounds of these distributions, our samples record ~3–6 Ma of total exposure and burial time. Rock surfaces likely underwent erosion at differing rates between samples and sites, but a rough indication of erosion rates at Skelton Glacier can be obtained by combining the results of all samples. During periods of exposure, the simulations estimate that the sampled surfaces were subjected to average subaerial erosion rates of ~0.4–0.6 m Ma^{-1} (**Fig. 6B**), similar to the rates estimated in the nearby Dry Valleys region (0.5–1.5 m/Ma, Balco et al., 2014; 0.7 m/Ma, Ivy-Ochs et al., 1995). During periods of ice cover, subglacial erosion likely occurred at average rates of ~0.7 m Ma^{-1} (**Fig. 6B**). Although, the magnitude of this basal erosion would have probably been much higher

towards the central flow path of the glacier where the ice is faster flowing and much thicker, with a far greater potential for basal melt and sliding (e.g. Golledge et al., 2013; Jones et al., 2016).

Modeling indicates that all nunatak sites experienced substantial burial by ice since the Pliocene. The simulated nuclide concentrations that were consistent with our data evolved primarily dependent on the duration of burial per glacial-interglacial cycle at each site, irrespective of total exposure-burial time and erosion rates. The duration of this burial per glacial-interglacial cycle correlates well with elevation above the modern ice surface (R^2 **≈** -0.91 to -0.99, $p < 0.03$ to < 0.001) (**Fig. 7**). At most sites, the relative duration of burial was broadly the same for the Pliocene, Early-Mid Pleistocene and Pliocene. The unnamed nunatak sample, collected within 2 m of the ice surface, implies that Skelton Glacier was thicker than present for 75–90% of a glacial-interglacial cycle (~75–90 ka per Late Pleistocene cycle, ~30–35 ka per Pliocene cycle, and ~30–35 ka or ~75–90 ka per Early-Mid Pleistocene cycle depending on the periodicity of the cycles). This is broadly consistent with the youngest exposure age collected at Halfway Nunatak, which implies at least ~6 ka of exposure over the last (100-ka) cycle. While the distribution of results is broader at Névé Nunatak, ~200 m above the modern ice surface, less burial time is predicted relative to the samples at lower elevation sites (**Fig. 7**). Here, our modeling suggests that ice cover likely occurred for ~35–95% and ~35–60% during Late and Early-Mid Pleistocene cycles, respectively, but just ~15–55% during Pliocene cycles. The modes and means of these probability distributions (at 45% and 47% for the Early-Mid Pleistocene, and 30% and 34% for the Pliocene, respectively) imply an apparent offset in the duration of ice cover per cycle, but the differences between the distributions are not significant at 68% confidence (**Fig. 7**). This result should therefore be considered with some caution.

Previous modeling of complex burial-exposure histories recognized that a higher $^{26}Al/^{10}Be$ production ratio can cause longer modeled burial durations (Corbett et al., 2016). We find that our data produce very similar results using a relatively high ratio of 7.28 (Borchers et al., 2016; scaling of Lifton et al., 2014) compared to the commonly accepted ratio of 6.75 that is applied here (**see supplementary data**).

4. Discussion

Cosmogenic nuclide data from rock surfaces at nunatak sites located across the Skelton Glacier catchment consist of two sample populations: 1) an erratic boulder with a relatively young ^{10}Be-derived exposure age of ~5.8 ka BP; and 2) 11 bedrock surfaces and erratic cobbles with much older and offset ^{10}Be- and ^{26}Al-derived apparent ages, and corresponding nuclide concentrations indicative of long-term exposure and burial histories. The former most likely represents deglaciation during the last glacial cycle and, as it is located close to the present-day glacier margin, implies that ice surface lowering here was near-complete by at least the mid-Holocene. However, this should only be considered as a tentative conclusion as it is based on just a single erratic sample, which could potentially have micro-inheritance (e.g. from incomplete surface erosion when last covered by ice (e.g. White et al., 2011)) or post-depositional alteration (e.g. subaerial erosion or movement following exposure). Consequently, this discussion focuses on the latter population, which records long-term exposure and burial of rock surfaces.

4.1. Old apparent ages and low $^{26}Al/^{10}Be$ ratios indicative of long-term exposure and burial

The majority of samples were shown to have nuclide concentrations requiring multi-stage exposure histories. This was evident as relatively old apparent exposure ages, which were significantly younger from ^{26}Al than from ^{10}Be. These apparent exposure ages increased

broadly with elevation of the sample site, reflecting greater cumulative exposure at higher elevations than at lower elevations. Preliminary evaluation of the concentrations identified that the $^{26}Al/^{10}Be$ ratios were largely inconsistent with continuous exposure and possible surface erosion. Instead, these concentrations implied at least ~150 ka to ~1.6 Ma of exposure and at least ~100 ka to ~850 ka of burial, assuming the simplistic scenario of an uninterrupted period of exposure and then burial. Notably, the amount of exposure and burial varied between sites and between the erratic cobbles. Discrete exposure-burial histories should be expected as each nunatak represents a slightly different part of the glacier catchment, each sample site has a different elevation relative to the modern ice surface, and all rock surfaces could have been subjected to varied degrees of erosion. Erratic cobbles additionally have the potential of a more diverse history, for example, from prior nuclide production at another site upstream and prolonged burial during glacial transport. While such differences can help explain the variance between sample concentrations, understanding the probable exposure-burial history at each site required systematic modeling, informed by the evidence of orbitally-paced ice margin oscillations recorded downstream of Skelton Glacier.

The primary outcomes of the modeling exercise, assuming that ice surface changes occurred over orbital frequencies, were that 1) the samples likely record a burial/exposure history since at least the Pliocene, 2) all sampled sites were buried during glacial periods, 3) the unnamed nunatak (lowest elevation) site was buried for ~75–90% of each glacial-interglacial cycle, and 4) burial at Névé Nunatak, the highest elevation site, possibly occurred for a relatively shorter time per Pliocene cycle than Pleistocene cycle. Apart from Névé Nunatak, where results were based on common exposure-burial histories of 7 erratic cobbles, the results for all other sites were based on single bedrock surface samples. In straightforward surface-exposure dating applications, multiple bedrock surfaces would be needed to provide a reliable representative age of a site or feature because of potential differential erosion rates

and prior exposure histories. Here, however, such effects were accounted for in the model, with the range of site elevations providing an additional tool to evaluate the reliability of these samples. The strong relationship between the duration of burial per glacial-interglacial cycle and the elevation of sample sites above the modern ice surface demonstrates that the samples suitably represent ice cover history at their respective sites.

In order to assume that the long-term exposure and burial histories that are implied by our data represent thinning and thickening of Skelton Glacier, we must rule out other possible causes. Nuclide decay associated with burial of a rock surface can occur from till or snow cover, or burial from local ice. It is unlikely that till or snow cover could explain our data as this cover would have to vary cyclically, probably in line with glacial-interglacial changes in climate, and have durations of cover stratigraphically consistent with elevation above the modern ice surface. Likewise, none of the nunatak sites are conducive to local glacier ice today or have topographic relief that might have facilitated local ice expansion in the past, particularly which was unrelated to Skelton Glacier.

There is also a possibility that changes in nuclide concentrations associated with burial/exposure may not have occurred over continuous glacial-interglacial cycles. For example, sites may have been continuously exposed during the Pliocene, prior to cycles of burial/exposure from a fluctuating ice surface during the Pleistocene. In our modeling, an ice-free Pliocene could occur with a scenario of 0% burial per Pliocene cycle, but the results showed that the nunatak sites were more likely partly ice-covered than completely exposed over this time (**Fig. 7**). While we cannot rule out other non-cyclic or missing cycle scenarios, the modeling exercise demonstrates that orbitally-paced ice surface histories, consistent with marine-based ice cover evidence, can explain the measured nuclide concentrations.

4.2. East Antarctic ice surface history since the Pliocene

Our analysis indicates that the surface of Skelton Glacier, connecting the East Antarctic plateau to the coastal ice margin, was higher than today during the Pliocene and Pleistocene. This is consistent with data from high altitude sites in the Transantarctic Mountains (e.g. Balco et al., 2014; Brook et al., 1993; Di Nicola et al., 2012; Fogwill et al., 2004; Staiger et al., 2006) and other East Antarctic sites representing surface elevation changes of the ice sheet interior (e.g. Lilly et al., 2010; Suganuma et al., 2014; Yamane et al., 2015), which suggest higher ice surface elevations potentially reflective of a thicker-than-present ice sheet during the Pliocene or at least the Early Pleistocene. Here, however, we find that thickening possibly occurred for a relatively shorter duration at high elevation sites in the Pliocene than in the Pleistocene, implying a general trend of increasing ice cover duration from the Pliocene towards present, rather than a progressively lowering ice surface over this time (e.g. Lilly et al., 2010; Yamane et al., 2015). The difference may reflect the location of the Skelton Glacier sites, at relatively lower elevations above the modern ice surface and in the mid-lower reaches of the glacier, closer to the influences of marine-based portions of the ice sheet. If so, our data analysis might imply that the surface of the ice sheet interior was higher during the Pliocene, but that outlet glaciers and the ice sheet margins had relatively higher surfaces during the Pleistocene.

Our analysis also indicates that the glacier surface elevation fluctuated substantially since at least the Pliocene. This is consistent with data collected at lower altitudes or nearer to the coast that show a complex surface-exposure history over this time (e.g. Balco et al., 2014; Di Nicola et al., 2009; Lilly et al., 2010), highlighting the magnitude of past surface elevation changes at areas akin to Skelton Glacier, upstream of the ice margin (**Fig. 8**).

4.3. Fluctuations of marine-based ice sheet margins

Fluctuations between contrasting glacial-interglacial ice surface elevations and outlet glacier configurations likely coincided with shifts in ice velocity and basal conditions through Pliocene and Pleistocene climates (**Fig. 8**). During glacial periods, ice sheet margins advanced towards the continental shelf edge (e.g. McKay et al., 2012; Naish et al., 2009; Patterson et al., 2014; Pollard and DeConto, 2009). The expansion of ice in the marine embayment acted as a buttress, restricting the flow of outlet glaciers and causing them to thicken upstream (e.g. Anderson et al., 2004; Denton and Hughes, 2000). At Skelton Glacier, the ice surface was probably at least 200 m higher than today during both Pliocene and Pleistocene glacial periods (**Fig. 7**), with greatest thickening likely occurring in the lower reaches of the glacier (Jones et al., 2016). While similar ice surface elevations are indicated by our data throughout this time at each site, progressive erosion of the bed beneath the central trunk of the glacier would mean that the corresponding ice thickness was likely greater in the Pleistocene than Pliocene (**Fig. 8**). These glacial periods lasted for 75–90% of a glacial-interglacial cycle, which is broadly consistent with estimates of glacial/interglacial durations inferred from paleoclimate records, at least for the Late Pleistocene (e.g. Tzedakis et al., 2012).

Interglacial periods are recorded at Skelton Glacier when the ice surface was likely near or below the present-day elevation, lasting for ~10–25% of a glacial-interglacial cycle. Although we are unable to constrain the magnitude of thinning during interglacial periods, glacier modeling predicts that the Skelton Glacier terminus could have retreated upstream of the overdeepened inlet, above sea level, under a Pliocene interglacial climate (Jones et al., 2016) (**Fig. 8**), which is similar to that modeled at Ferrar Glacier, another East Antarctic outlet glacier (Golledge and Levy, 2011). Warm sea surface (+3–5 °C) (Winter et al., 2010) and atmospheric temperatures in the Pliocene likely also produced a more dynamic glacier

profile with enhanced basal erosion and offshore sediment deposition, relative to that in the Pleistocene (**Fig. 8**) (Levy et al., 2012). At times when the vicinity downstream of Skelton Glacier was open water (Naish et al., 2009), continent-scale ice sheet modeling indicates that significant deglaciation of the WAIS, and the Wilkes Basin in East Antarctica, occurred (Austermann et al., 2015; Pollard and DeConto, 2009). Recent ice sheet simulations indicate that substantial retreat of the EAIS and WAIS margins possibly also occurred during the Pleistocene (DeConto and Pollard, 2016). This is consistent with our data from Skelton Glacier, which shows that the duration of deglaciation, relative to glacial expansion, was similar in both the Pliocene and Pleistocene.

Large amplitude glacial-interglacial fluctuations of the glacier surface and ice sheet margin are inferred despite there being contrasting climates between the Pliocene and Pleistocene. Relatively high precipitation during the Pliocene, possibly from increased moisture transport (Yamane et al., 2015), could have caused greater thickening of the ice sheet interior. Meanwhile, the relatively warmer air and ocean temperatures (Haywood et al., 2013; Winter et al., 2010) would have facilitated more extensive basal sliding and higher surface velocities of East Antarctic outlet glaciers (Golledge and Levy, 2011; Jones et al., 2016; Levy et al., 2012), allowing for oscillations of the ice margin and the faster propagation of ice flux changes inland (**Fig. 8**). The climate cooled globally towards the Late Pleistocene, helping ice sheets to thicken and advance during glacial periods (**Fig. 8**). Progressive glacial incision of bedrock troughs and basins on the continental shelf since the Late Pliocene (Golledge et al., 2013; Rebesco and Camerlenghi, 2008) would have allowed deglaciation to occur during Pleistocene interglacial periods from enhanced marine instability feedbacks and only moderately warm temperatures. In locations where multiple outlet glaciers and ice streams coalesced in an embayment, such as the Ross Embayment, buttressing effects likely

acted to amplify the upstream thickening of glaciers during Pliocene and Pleistocene glacial periods.

5. Conclusions

We applied multiple-isotope cosmogenic nuclide analysis to cobble and bedrock surface samples, collected at ice-free sites flanking Skelton Glacier, in order to record a history of ice surface fluctuations. While one boulder possibly indicates that relatively recent deglaciation was near-complete by the mid-Holocene, all other samples (11 of 12) provide much older ^{10}Be- and ^{26}Al-derived apparent ages, and corresponding nuclide concentrations indicative of long-term exposure and burial histories. We assume that exposure and burial occurred over glacial-interglacial cycles, driven by orbital cycles that are reflected in benthic oxygen isotopes and local Antarctic ice marginal sediments. By modeling nuclide concentrations through these glacial-interglacial cycles, we identified the most probable glacier surface fluctuation histories that are consistent with our data. Firstly, relatively low erosion rates of a few decimeters per Ma have preserved long-term exposure histories in these samples, which imply substantial exposure and burial since at least the Pliocene. Secondly, the ice surface was likely >200 m higher than today during glacial periods, covering our highest elevation site, and the glacier has probably been thicker than present for ~75–90% of each glacial-interglacial cycle. Thirdly, ice cover at higher elevations possibly occurred for a relatively shorter time per Pliocene cycle than Pleistocene cycle. While it is not possible to determine the magnitude of surface lowering during interglacial periods, our data imply that the duration of deglaciation, relative to glacial expansion, was similar in both the Pliocene and Pleistocene.

Our analysis links new onshore data of ice surface elevations from an East Antarctic outlet glacier with offshore evidence of the ice margin that is recorded downstream of the

study area. The outcomes are consistent with evidence from the edge of the East Antarctic plateau that indicate a higher ice sheet surface existed during the Pliocene, but also highlight that glacier surface elevations fluctuated substantially since the Pliocene. Large glacial-interglacial fluctuations in ice extent occurred at the marine-based ice margin of the East Antarctic Ice Sheet, in response to the evolving climate and bed topography since at least the Pliocene. Over this time, we have shown how such changes can be manifested upstream as surface elevation changes of outlet glaciers. The scale of these ice surface fluctuations during the Pliocene and Pleistocene can be used to better inform ice sheet models that simulate long-term ice volume, and corresponding sea level contribution, over glacial-interglacial cycles.

Acknowledgements

This work was supported by the MBIE Past Antarctic Climate and Future Implications program (Impact Statement 1 'Response of the Antarctic Ice Sheet to transient climate change', A.N.M., G.S.W. and N.R.G.). Additionally, R.S.J. was supported by a Victoria Doctoral Scholarship and New Zealand Antarctic Research Institute grant. We acknowledge field support from Antarctica New Zealand, which was funded by the New Zealand Government (MBIE) contract C05X1001 to G.S.W. J.T.H.A. was supported by an Australian Institute of Nuclear Science and Engineering (AINSE) Postgraduate award (10925) and a University of Otago departmental award. Sample preparation and measurements were made possible by Antarctic Science Bursary and AINSE (09015) grants. We thank B. Dagg and A. Cole for help in the field, and T. Naish, M. Bentley and three anonymous reviewers for constructive comments that improved this paper.

References

Ackert, R.P., Barclay, D.J., Borns, H.W., Calkin, P.E., Kurz, M.D., Fastook, J.L., Steig, E.J., 1999. Measurements of past ice sheet elevations in interior West Antarctica. Science 286, 276-280.

Anderson, B.M., Hindmarsh, R.C.A., Lawson, W.J., 2004. A modelling study of the response of Hatherton Glacier to Ross Ice Sheet grounding line retreat. Global and Planetary Change 42, 143-153.

Austermann, J., Pollard, D., Mitrovica, J.X., Moucha, R., Forte, A.M., DeConto, R.M., Rowley, D.B., Raymo, M.E., 2015. The impact of dynamic topography change on Antarctic ice sheet stability during the mid-Pliocene warm period. Geology 43, 927-930.

Balco, G., Shuster, D.L., 2009. Production rate of cosmogenic ^{21}Ne in quartz estimated from ^{10}Be, ^{26}Al, and ^{21}Ne concentrations in slowly eroding Antarctic bedrock surfaces. Earth and Planetary Science Letters 281, 48-58.

Balco, G., Stone, J.O., Lifton, N.A., Dunai, T.J., 2008. A complete and easily accessible means of calculating surface exposure ages or erosion rates from ^{10}Be and ^{26}Al measurements. Quaternary Geochronology 3, 174-195.

Balco, G., Stone, J.O.H., Sliwinski, M.G., Todd, C., 2014. Features of the glacial history of the Transantarctic Mountains inferred from cosmogenic ^{26}Al, ^{10}Be and ^{21}Ne concentrations in bedrock surfaces. Antarctic Science 26, 708-723.

Bierman, P.R., Marsella, K.A., Patterson, C., Davis, P.T., Caffee, M., 1999. Mid-Pleistocene cosmogenic minimum-age limits for pre-Wisconsinan glacial surfaces in southwestern Minnesota and southern Baffin Island: a multiple nuclide approach. Geomorphology 27, 25-39.

Borchers, B., Marrero, S., Balco, G., Caffee, M., Goehring, B., Lifton, N., Nishiizumi, K., Phillips, F., Schaefer, J., Stone, J., 2016. Geological calibration of spallation production rates in the CRONUS-Earth project. Quaternary Geochronology 31, 188-198.

Briner, J.P., Miller, G.H., Davis, P.T., Finkel, R.C., 2006. Cosmogenic radionuclides from fiord landscapes support differential erosion by overriding ice sheets. Geological Society of America Bulletin 118, 406-420.

Brook, E.J., Kurz, M.D., Ackert, R.P., Denton, G.H., Brown, E.T., Raisbeck, G.M., Yiou, F., 1993. Chronology of Taylor Glacier advances in Arena Valley, Antarctica, using in situ cosmogenic ^{3}He and ^{10}Be. Quaternary Research 39, 11-23.

Chmeleff, J., von Blanckenburg, F., Kossert, K., Jakob, D., 2010. Determination of the ^{10}Be half-life by multicollector ICP-MS and liquid scintillation counting. Nuclear Instruments and Methods in Physics Research Section B: Beam Interactions with Materials and Atoms 268, 192-199.

Corbett, L.B., Bierman, P.R., Rood, D.H., 2016. Constraining multi-stage exposure-burial scenarios for boulders preserved beneath cold-based glacial ice in Thule, northwest Greenland. Earth and Planetary Science Letters 440, 147-157.

DeConto, R.M., Pollard, D., 2016. Contribution of Antarctica to past and future sea-level rise. Nature 531, 591-597.

Denton, G.H., Hughes, T.J., 2000. Reconstruction of the Ross ice drainage system, Antarctica, at the last glacial maximum. Geografiska Annaler: Series A, Physical Geography 82, 143-166.

Di Nicola, L., Baroni, C., Strasky, S., Salvatore, M.C., Schlüchter, C., Akçar, N., Kubik, P.W., Wieler, R., 2012. Multiple cosmogenic nuclides document the stability of the East Antarctic Ice Sheet in northern Victoria Land since the Late Miocene (5–7 Ma). Quaternary Science Reviews 57, 85-94.

Di Nicola, L., Strasky, S., Schlüchter, C., Salvatore, M.C., Akçar, N., Kubik, P.W., Christl, M., Kasper, H.U., Wieler, R., Baroni, C., 2009. Multiple cosmogenic nuclides document complex Pleistocene exposure history of glacial drifts in Terra Nova Bay (northern Victoria Land, Antarctica). Quaternary Research 71, 83-92.

Fogwill, C.J., Bentley, M.J., Sugden, D.E., Kerr, A.R., Kubik, P.W., 2004. Cosmogenic nuclides ^{10}Be and ^{26}Al imply limited Antarctic Ice Sheet thickening and low erosion in the Shackleton Range for >1 m.y. Geology 32, 265.

Golledge, N.R., Levy, R.H., 2011. Geometry and dynamics of an East Antarctic Ice Sheet outlet glacier, under past and present climates. Journal of Geophysical Research 116.

Golledge, N.R., Levy, R.H., McKay, R.M., Fogwill, C.J., White, D.A., Graham, A.G.C., Smith, J.A., Hillenbrand, C.-D., Licht, K.J., Denton, G.H., Ackert, R.P., Maas, S.M., Hall, B.L., 2013. Glaciology and geological signature of the Last Glacial Maximum Antarctic ice sheet. Quaternary Science Reviews 78, 225-247.

Gunn, B.M., Warren, G., 1962. Geology of Victoria Land between the Mawson and Mulock Glaciers, Antarctica. Trans-antarctic expedition Committee.

Haywood, A.M., Hill, D.J., Dolan, A.M., Otto-Bliesner, B.L., Bragg, F., Chan, W.L., Chandler, M.A., Contoux, C., Dowsett, H.J., Jost, A., Kamae, Y., Lohmann, G., Lunt, D.J., Abe-Ouchi, A., Pickering, S.J., Ramstein, G., Rosenbloom, N.A., Salzmann, U., Sohl, L., Stepanek, C., Ueda, H., Yan, Q., Zhang, Z., 2013. Large-scale features of Pliocene climate: results from the Pliocene Model Intercomparison Project. Climate of the Past 9, 191-209.

Ivy-Ochs, S., Schlüchter, C., Kubik, P.W., Dittrich-Hannen, B., Beer, J., 1995. Minimum ^{10}Be exposure ages of early Pliocene for the Table Mountain plateau and the Sirius Group at Mount Fleming, Dry Valleys, Antarctica. Geology 23, 1007-1010.

Jones, R., Golledge, N., Mackintosh, A., Norton, K., 2016. Past and present dynamics of Skelton Glacier, Transantarctic Mountains. Antarctic Science 28, 371-386.

Korschinek, G., Bergmaier, A., Faestermann, T., Gerstmann, U.C., Knie, K., Rugel, G., Wallner, A., Dillmann, I., Dollinger, G., von Gostomski, C.L., Kossert, K., Maiti, M., Poutivtsev, M., Remmert, A., 2010. A new value for the half-life of ^{10}Be by Heavy-Ion Elastic Recoil Detection and liquid scintillation counting. Nuclear Instruments and Methods in Physics Research Section B: Beam Interactions with Materials and Atoms 268, 187-191.

Lal, D., 1991. Cosmic ray labeling of erosion surfaces: in situ nuclide production rates and erosion models. Earth and Planetary Science Letters 104, 424-439.

Levy, R., Cody, R., Crampton, J., Fielding, C., Golledge, N., Harwood, D., Henrys, S., McKay, R., Naish, T., Ohneiser, C., Wilson, G., Wilson, T., Winter, D., 2012. Late Neogene climate and glacial history of the Southern Victoria Land coast from integrated drill core, seismic and outcrop data. Global and Planetary Change 96-97, 157-180.

Lifton, N., Sato, T., Dunai, T.J., 2014. Scaling in situ cosmogenic nuclide production rates using analytical approximations to atmospheric cosmic-ray fluxes. Earth and Planetary Science Letters 386, 149-160.

Lilly, K., Fink, D., Fabel, D., Lambeck, K., 2010. Pleistocene dynamics of the interior East Antarctic ice sheet. Geology 38, 703-706.

Lisiecki, L.E., Raymo, M.E., 2005. A Pliocene-Pleistocene stack of 57 globally distributed benthic δ^{18}O records. Paleoceanography 20.

McKay, R., Naish, T., Powell, R., Barrett, P., Scherer, R., Talarico, F., Kyle, P., Monien, D., Kuhn, G., Jackolski, C., Williams, T., 2012. Pleistocene variability of Antarctic Ice Sheet extent in the Ross Embayment. Quaternary Science Reviews 34, 93-112.

Mifsud, C., Fujioka, T., Fink, D., 2013. Extraction and purification of quartz in rock using hot phosphoric acid for in situ cosmogenic exposure dating. Nuclear Instruments and

Methods in Physics Research Section B: Beam Interactions with Materials and Atoms 294, 203-207.
Naish, T., Powell, R., Levy, R., Wilson, G., Scherer, R., Talarico, F., Krissek, L., Niessen, F., Pompilio, M., Wilson, T., Carter, L., DeConto, R., Huybers, P., McKay, R., Pollard, D., Ross, J., Winter, D., Barrett, P., Browne, G., Cody, R., Cowan, E., Crampton, J., Dunbar, G., Dunbar, N., Florindo, F., Gebhardt, C., Graham, I., Hannah, M., Hansaraj, D., Harwood, D., Helling, D., Henrys, S., Hinnov, L., Kuhn, G., Kyle, P., Laufer, A., Maffioli, P., Magens, D., Mandernack, K., McIntosh, W., Millan, C., Morin, R., Ohneiser, C., Paulsen, T., Persico, D., Raine, I., Reed, J., Riesselman, C., Sagnotti, L., Schmitt, D., Sjunneskog, C., Strong, P., Taviani, M., Vogel, S., Wilch, T., Williams, T., 2009. Obliquity-paced Pliocene West Antarctic ice sheet oscillations. Nature 458, 322-328.
Nishiizumi, K., 2004. Preparation of 26 Al AMS standards. Nuclear Instruments and Methods in Physics Research Section B: Beam Interactions with Materials and Atoms 223, 388-392.
Nishiizumi, K., Imamura, M., Caffee, M.W., Southon, J.R., Finkel, R.C., McAninch, J., 2007. Absolute calibration of ^{10}Be AMS standards. Nuclear Instruments and Methods in Physics Research Section B: Beam Interactions with Materials and Atoms 258, 403-413.
Norton, K.P., von Blanckenburg, F., Schlunegger, F., Schwab, M., Kubik, P.W., 2008. Cosmogenic nuclide-based investigation of spatial erosion and hillslope channel coupling in the transient foreland of the Swiss Alps. Geomorphology 95, 474-486.
Patterson, M.O., McKay, R., Naish, T., Escutia, C., Jimenez-Espejo, F.J., Raymo, M.E., Meyers, S.R., Tauxe, L., Brinkhuis, H., Klaus, A., Fehr, A., Bendle, J.A.P., Bijl, P.K., Bohaty, S.M., Carr, S.A., Dunbar, R.B., Flores, J.A., Gonzalez, J.J., Hayden, T.G., Iwai, M., Katsuki, K., Kong, G.S., Nakai, M., Olney, M.P., Passchier, S., Pekar, S.F., Pross, J., Riesselman, C.R., Röhl, U., Sakai, T., Shrivastava, P.K., Stickley, C.E., Sugasaki, S., Tuo, S., van de Flierdt, T., Welsh, K., Williams, T., Yamane, M., 2014. Orbital forcing of the East Antarctic ice sheet during the Pliocene and Early Pleistocene. Nature Geoscience 7, 841-847.
Pollard, D., DeConto, R.M., 2009. Modelling West Antarctic ice sheet growth and collapse through the past five million years. Nature 458, 329-332.
Rebesco, M., Camerlenghi, A., 2008. Late Pliocene margin development and mega debris flow deposits on the Antarctic continental margins: Evidence of the onset of the modern Antarctic Ice Sheet? Palaeogeography, Palaeoclimatology, Palaeoecology 260, 149-167.
Rignot, E., Mouginot, J., Scheuchl, B., 2011. Ice flow of the Antarctic ice sheet. Science 333, 1427-1430.
Staiger, J.W., Marchant, D.R., Schaefer, J.M., Oberholzer, P., Johnson, J.V., Lewis, A.R., Swanger, K.M., 2006. Plio-Pleistocene history of Ferrar Glacier, Antarctica: Implications for climate and ice sheet stability. Earth and Planetary Science Letters 243, 489-503.
Stone, J.O., 2000. Air pressure and cosmogenic isotope production. Journal of Geophysical Research: Solid Earth (1978–2012) 105, 23753-23759.
Stone, J.O., Balco, G.A., Sugden, D.E., Caffee, M.W., Sass, L.C., Cowdery, S.G., Siddoway, C., 2003. Holocene deglaciation of Marie Byrd land, west Antarctica. Science 299, 99-102.
Suganuma, Y., Miura, H., Zondervan, A., Okuno, J.i., 2014. East Antarctic deglaciation and the link to global cooling during the Quaternary: evidence from glacial geomorphology and ^{10}Be surface exposure dating of the Sør Rondane Mountains, Dronning Maud Land. Quaternary Science Reviews 97, 102-120.

Sugden, D.E., Balco, G., Cowdery, S.G., Stone, J.O., Sass, L.C., 2005. Selective glacial erosion and weathering zones in the coastal mountains of Marie Byrd Land, Antarctica. Geomorphology 67, 317-334.

Talarico, F.M., McKay, R.M., Powell, R.D., Sandroni, S., Naish, T., 2012. Late Cenozoic oscillations of Antarctic ice sheets revealed by provenance of basement clasts and grain detrital modes in ANDRILL core AND-1B. Global and Planetary Change 96-97, 23-40.

Tzedakis, P.C., Wolff, E.W., Skinner, L.C., Brovkin, V., Hodell, D.A., McManus, J.F., Raynaud, D., 2012. Can we predict the duration of an interglacial? Climate of the Past 8, 1473-1485.

Von Blanckenburg, F., Belshaw, N., O'Nions, R., 1996. Separation of ^{9}Be and cosmogenic ^{10}Be from environmental materials and SIMS isotope dilution analysis. Chemical Geology 129, 93-99.

White, D., Fülöp, R.-H., Bishop, P., Mackintosh, A., Cook, G., 2011. Can in-situ cosmogenic ^{14}C be used to assess the influence of clast recycling on exposure dating of ice retreat in Antarctica? Quaternary Geochronology 6, 289-294.

Winter, D., Sjunneskog, C., Harwood, D., 2010. Early to mid-Pliocene environmentally constrained diatom assemblages from the AND-1B drillcore, McMurdo Sound, Antarctica. Stratigraphy 7, 207.

Yamane, M., Yokoyama, Y., Abe-Ouchi, A., Obrochta, S., Saito, F., Moriwaki, K., Matsuzaki, H., 2015. Exposure age and ice-sheet model constraints on Pliocene East Antarctic ice sheet dynamics. Nature Communications 6, 7016.

Tables

Table 1. Nuclide concentrations.

Site	Sample ID	Final quartz weight (g)	Mass of ^{9}Be added (mg)	^{10}Be conc. (atoms g^{-1})	^{10}Be conc. 1 sigma (atoms g^{-1})	^{26}Al conc. (atoms g^{-1})	^{26}Al conc. 1 sigma (atoms g^{-1})	^{26}Al/^{10}Be ratio	Ratio 1 sigma
Unnamed Nunatak	AN35 *	61.03	0.1784	2.13E+06	6.38E+04	1.10E+07	6.47E+05	5.16	0.50
Halfway Nunatak	HN36 *	21.54	0.1650	7.47E+04	7.60E+03	–	–	–	–
Escalade-Tate Peak saddle	EP26 †	50.08	0.3810	5.21E+06	1.31E+05	2.35E+07	1.60E+06	4.51	0.47
Tate Peak	EP25 †	50.06	0.3840	5.57E+06	1.28E+05	2.99E+07	1.20E+06	5.37	0.37
Clinker Bluff	CB38 *	33.80	0.2055	6.73E+06	1.61E+05	2.63E+07	1.17E+06	3.91	0.29
Névé Nunatak	NN33d *	12.30	0.1677	1.05E+07	3.14E+05	5.41E+07	1.49E+06	5.16	0.31
Névé Nunatak	NN33c *	57.40	0.1677	8.18E+06	2.62E+05	4.48E+07	5.35E+05	5.48	0.28
Névé Nunatak	NN31 *	26.40	0.1680	1.44E+07	4.33E+05	5.46E+07	9.93E+05	3.79	0.20
Névé Nunatak	NN32 *	34.02	0.1672	5.19E+06	1.56E+05	2.72E+07	1.10E+06	5.23	0.38
Névé Nunatak	NN33a *	36.89	0.1681	1.04E+07	3.13E+05	5.30E+07	2.48E+05	5.08	0.22
Névé Nunatak	NN33b *	56.75	0.1677	1.05E+07	3.14E+05	5.23E+07	1.91E+06	4.99	0.35
Névé Nunatak	NN30 *	56.24	0.1861	1.45E+07	4.36E+05	6.25E+07	2.05E+06	4.30	0.29

Samples were processed at *VUW and †ANSTO, and measured at ETH Zurich/GFZ and ANSTO, respectively (see text).

Table 2. Apparent exposure ages.

Nunatak	Sample ID	^{10}Be age (ka)			^{26}Al age (ka)			P_s (atoms g^{-1} a^{-1})	
		Mean age	1 sigma (internal)	1 sigma (external)	Mean age	1 sigma (internal)	1 sigma (external)	^{10}Be	^{26}Al
Unnamed nunatak	AN35	121	4	11	94	6	10	17.77	119.88
Halfway Nunatak	HN36	5.8	0.6	0.8	–	–	–	12.72	–
Escalade-Tate Peak saddle	EP26	257	7	25	175	13	21	21.28	143.55
Tate Peak	EP25	288	7	28	238	11	26	20.47	138.10
Clinker Bluff	CB38	815	24	91	484	28	61	9.81	66.18
Névé Nunatak	NN33d	660	23	72	557	20	68	18.32	123.60
Névé Nunatak	NN33c	489	18	51	430	6	47	18.55	125.17
Névé Nunatak	NN31	971	38	115	559	14	66	18.43	124.32
Névé Nunatak	NN32	290	9	29	234	11	25	18.93	127.72
Névé Nunatak	NN33a	658	23	72	541	3	62	18.33	123.67
Névé Nunatak	NN33b	657	23	71	529	25	65	18.40	124.12
Névé Nunatak	NN30	955	37	113	656	30	86	18.78	126.68

P_S = Sample-specific production rate for spallation.
Exposure ages are calculated using the Lal/Stone scheme (Lal, 1991; Stone, 2000).
'Internal' refers to solely the measurement uncertainty of the nuclide measurement, while the 'external' uncertainty additionally includes production rate uncertainties.

Figure Captions

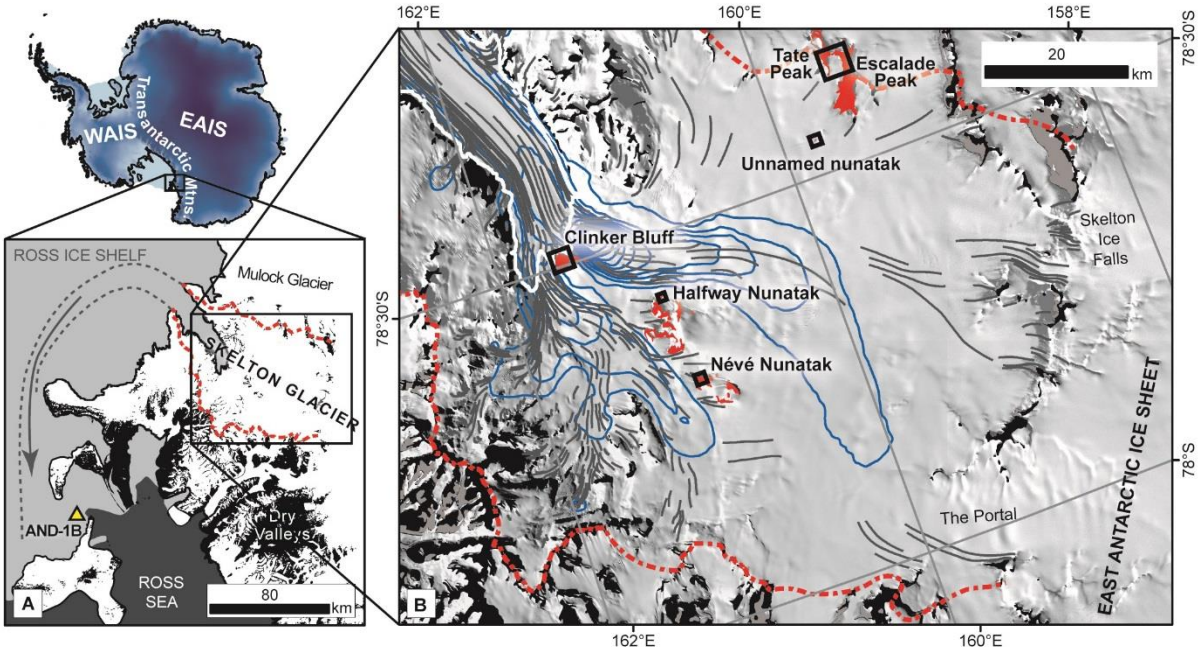

Figure 1. Study area context. A) Skelton Glacier delivers ice from the East Antarctic Ice Sheet (EAIS) to the Ross Sea and AND-1B core site (yellow triangle; Naish et al., 2009) today, indicated by an arrow, and likely has done since at least the Pliocene (Talarico et al., 2012). Ice-free areas are shown in black. WAIS – West Antarctic Ice Sheet. B) Nunataks targeted for surface-exposure analysis are in red (boxed sample sites are shown in Figure 2). The catchment boundary of Skelton Glacier (as defined in Jones et al., 2016) is denoted with a red dot-dashed line, while ice flow is highlighted with mapped flow stripes (grey lines) and ice velocity contours (blue lines at 25 m a^{-1} intervals; Rignot et al., 2011).

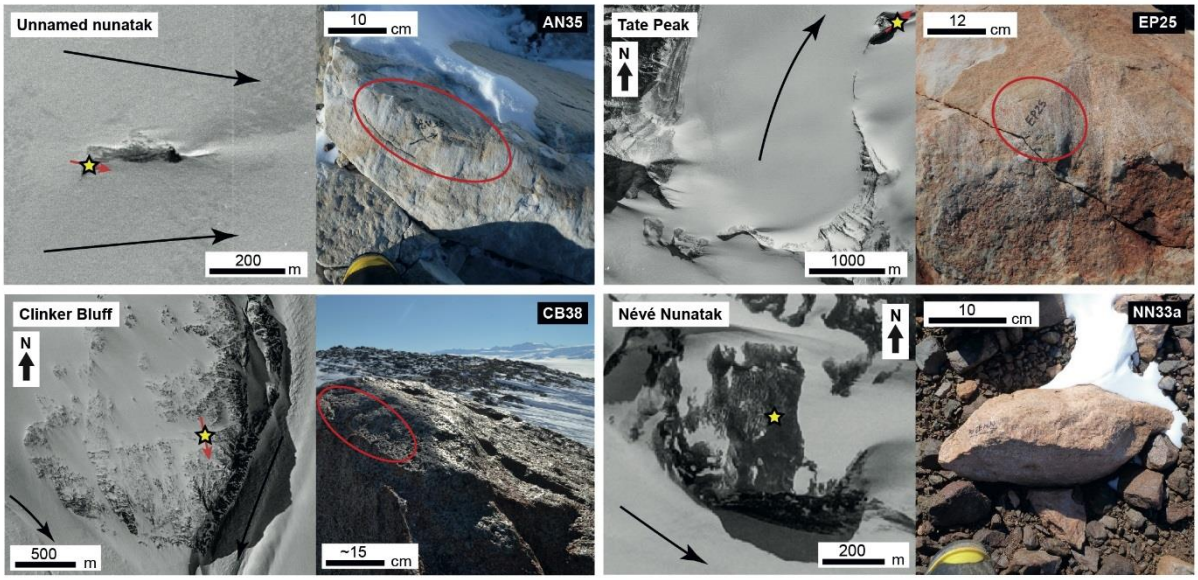

Figure 2. Four example samples collected at Skelton Glacier nunataks. The location of each sample is shown by a yellow star on an aerial photograph. Black arrows highlight the modern ice flow direction, while red arrows denote the former ice flow, apparent from bedrock striae where available. The details of all samples are provided in the supplement.

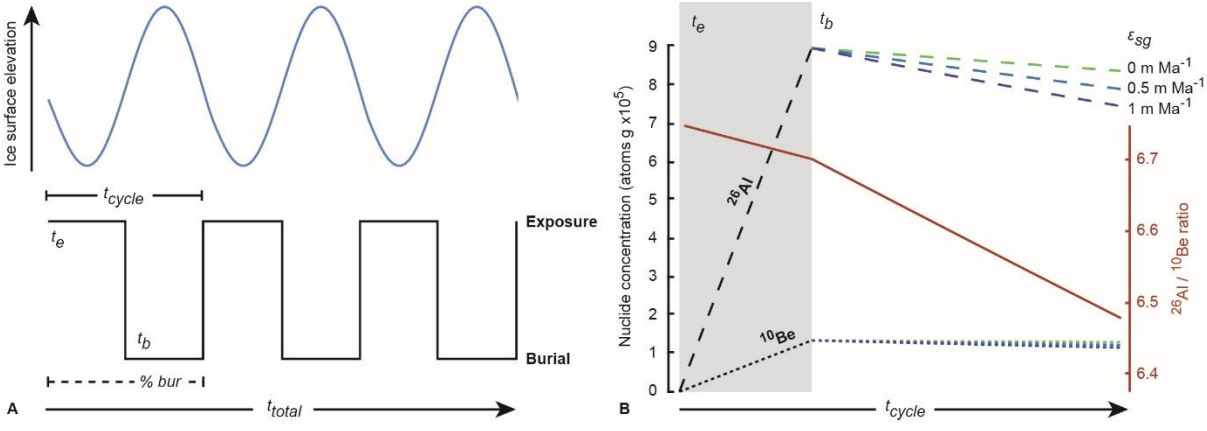

Figure 3. Summary of exposure-burial modeling approach used. A) Nuclide production and decay is calculated for episodes of exposure (t_e) and burial (t_b) through glacial-interglacial cycles (t_{cycle}), for an assigned period of time (t_{total}). The percent of ice cover per cycle ($\%\ bur$) determines the duration of t_e and t_b. B) Concentrations of ^{10}Be and ^{26}Al are produced and then decay over an exposure-burial cycle (calculated here for t_e 30 ka, t_b 70

ka). Higher erosion rates increase the amount of nuclide loss, shown here for subglacial erosion (ε_{sg}) during burial by ice.

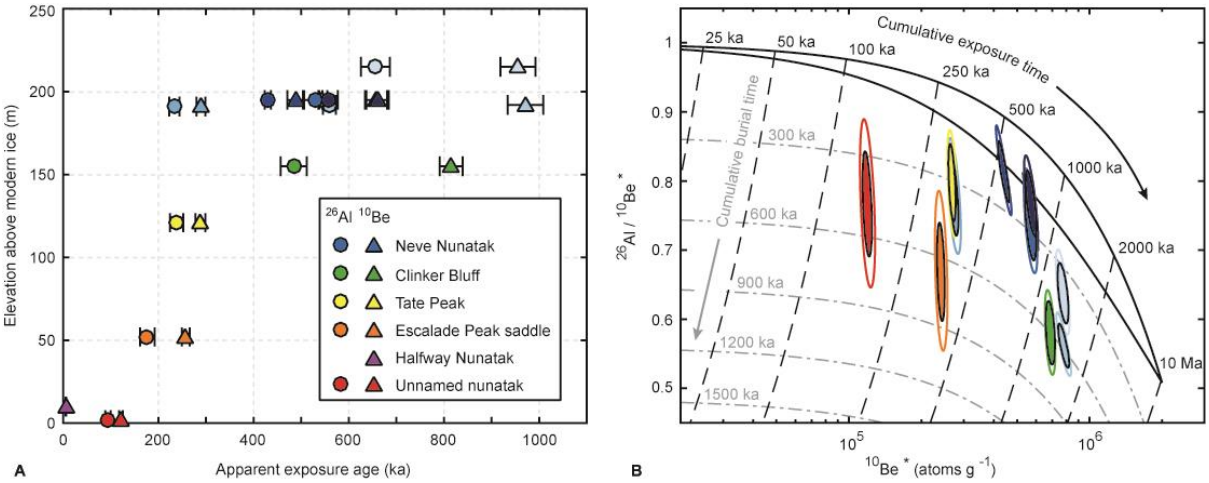

Figure 4. Measured burial/exposure history of the samples. A) Apparent exposure ages are based on ^{10}Be and ^{26}Al concentrations (Tables 1 and 2) and shown for each sample site with measurement uncertainty (68% confidence). B) The corresponding sample concentrations (normalized; 68% and 95% confidence) are shown as ellipses on a two-isotope plot, with burial (dot-dashed lines) and exposure (dashed lines) isochrones, and the steady-state erosion island (solid black lines).

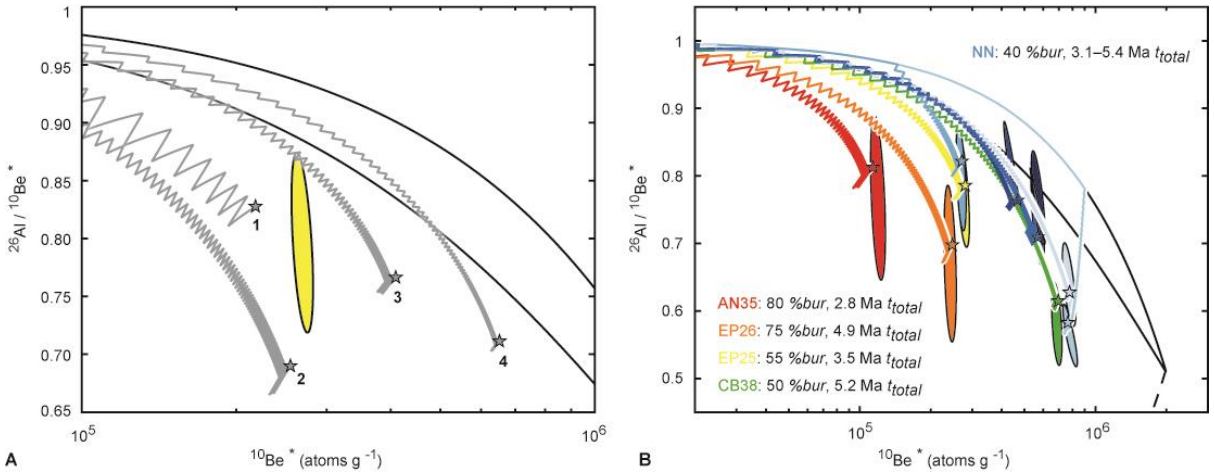

Figure 5. Simulated exposure-burial scenarios shown on a two-isotope plot (see Fig. 4B). Nuclide concentrations evolve through glacial-interglacial cycles, with each pathway dependent on the periodicity of cycles, percent of each cycle covered by ice (% bur), total time of cycles (t_{total}), and subglacial (ε_{sg}) and subaerial (ε_{sa}) erosion rates. A) Example scenarios where the final nuclide concentrations were not consistent with sample EP25 (at 95% confidence), and were therefore rejected: 1) 1.2 Ma t_{total}, 65 % bur, 0.5 m Ma^{-1} ε_{sg}, 0.5 m Ma^{-1} ε_{sa}, 2) 4.8 Ma t_{total}, 85 % bur, 0.1 m Ma^{-1} ε_{sg}, 0.6 m Ma^{-1} ε_{sa}, 3) 3.5 Ma t_{total}, 40 % bur, 0.6 m Ma^{-1} ε_{sg}, 0.6 m Ma^{-1} ε_{sa}, 4) 5.4 Ma t_{total}, 20 % bur, 0.3 m Ma^{-1} ε_{sg}, 0.3 m Ma^{-1} ε_{sa}. B) Example scenarios that converge with our data, and were therefore accepted. Note the change in axes scale. As the erratic cobble samples at Névé Nunatak (NN) were allowed to evolve from constant exposure prior to cyclic exposure-burial, two such scenarios are included in this plot. Sample concentrations are plotted as ellipses for 95% probability.

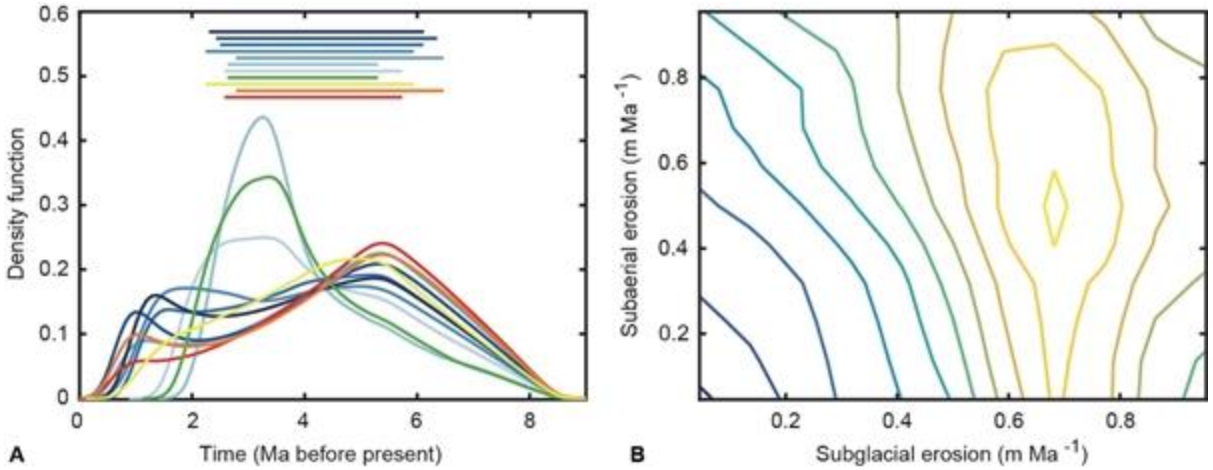

Figure 6. Modeled probable burial/exposure histories that explain the measured nuclide concentrations. A) Probability density estimates for each sample (individual line colors correspond to samples as in Fig. 4), where the peak of a curve (mode) reflects the highest likelihood. Based on these modes, rock surfaces most likely record first exposure between ~3 and 6 Ma BP; a few samples at Névé Nunatak and Tate Peak were possibly first exposed at ~1–2 Ma BP. The 68% confidence bounds of these distributions are also shown as horizontal bars. B) Erosion rates over this time are shown for subaerial vs. subglacial erosion, with contours colored blue (low probability) to yellow (high probability). Subaerial erosion most likely occurred at ~0.4–0.6 m Ma^{-1}, while subglacial erosion occurred at ~0.7 m Ma^{-1}, on average across the catchment.

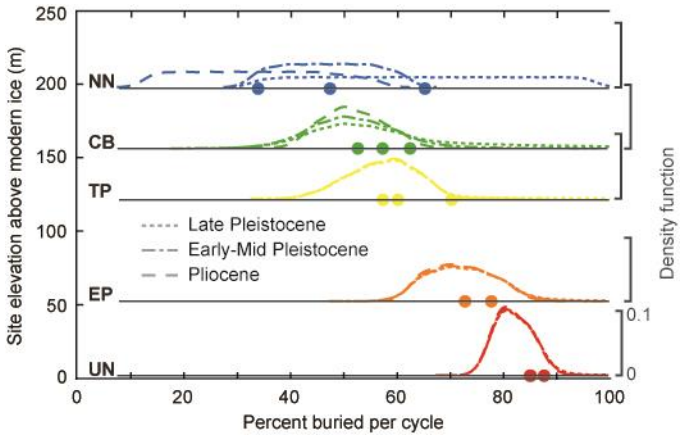

Figure 7. Ice cover per glacial-interglacial cycle. The modeled percent buried per cycle is shown as probability density estimates for each nunatak, with the means of each distribution as filled circles. The duration of ice cover is well correlated with elevation of the site above the modern ice surface; linear regression analysis of the means determines an r^2 of -0.9132 ($p = 0.0282$) for the Late Pleistocene, -0.9927 ($p = 0.0008$) for the Early-Mid Pleistocene, and -0.9793 ($p = 0.0036$) for the Pliocene. At Névé Nunatak (NN), the probability distributions of ice cover per cycle differ between the Pliocene (mode 30%, mean 34%) and Early-Mid Pleistocene (mode 45%, mean 47%).

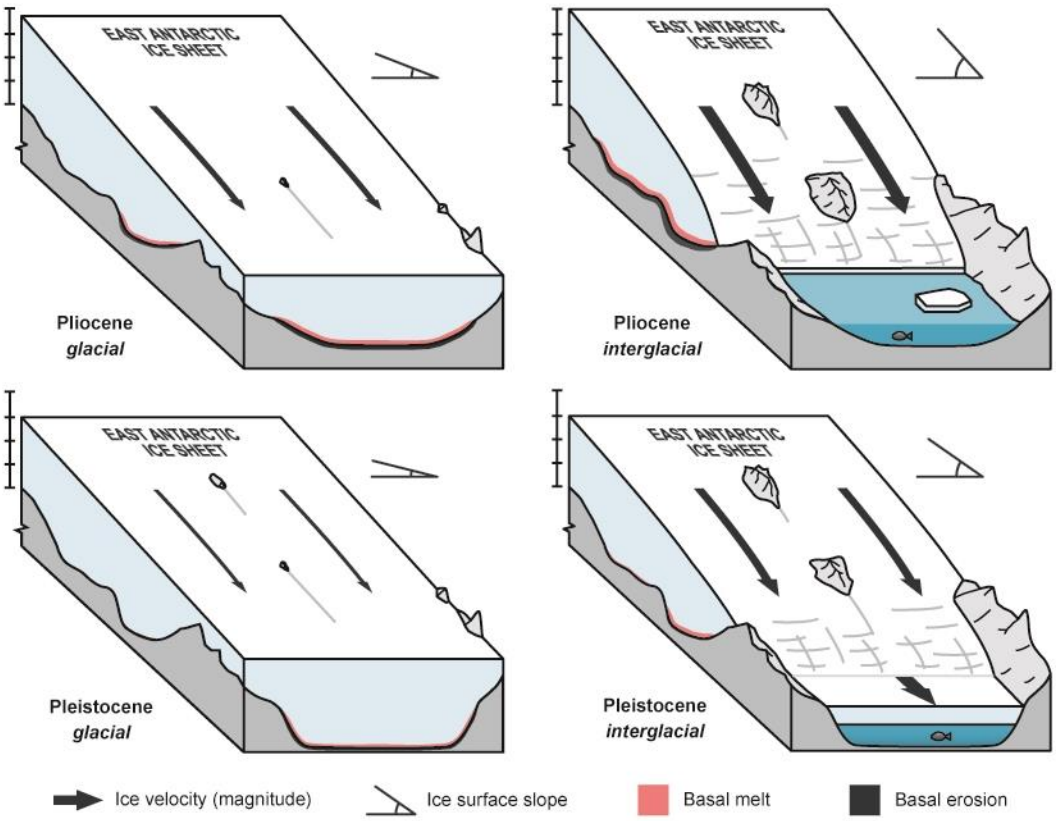

Figure 8. Conceptual reconstruction of outlet glacier configurations during the Pliocene and Pleistocene. Ice surface elevation, relative ice surface slope and velocity, potential for basal melt and glacial incision, and terminus position are based on our new and previously published (e.g. Yamane et al., 2015) ice surface elevation data, as well as simulations of East Antarctic outlet glaciers under past climates (Golledge and Levy, 2011; Jones et al., 2016).